Precise in-situ measurement of laser pulse intensity using strong field ionization

Smeenk, C.; Salvail, J. Z.; Arissian, L.; Corkum, P. B.; Hebeisen, C. T.; Staudte, A.

Publisher's version / Version de l'éditeur:
http://dx.doi.org/10.1364/OE.19.009336
Optics Express, 19, p. 9336, 2011

Precise *in-situ* measurement of laser pulse intensity using strong field ionization

C. Smeenk,[1,*] **J. Z. Salvail,**[1] **L. Arissian,**[1,2,3] **P. B. Corkum,**[1] **C. T. Hebeisen,**[1] **and A. Staudte**[1]

[1] *Joint Laboratory for Attosecond Science, University of Ottawa and National Research Council, 100 Sussex Drive, Ottawa, Canada*
[2] *Department of Physics, University of New Mexico, Albuquerque, New Mexico, USA*
[3] *Department of Physics, Texas A & M University, College Station, Texas, USA*

[*] *christopher.smeenk@nrc.ca*

Abstract: Building on the work of Alnaser et al. [Phys. Rev. A 70, 023413 (2004)], we devise an improved method for an *in-situ* measurement of the peak intensity in a focused, femtosecond infrared laser pulse. The method is shown to be effective with both photoion and photoelectron imaging devices. The model used to fit the experimental data has no unphysical free parameters used in fitting. The accuracy of the fit is 4% and the overall accuracy of the measurement is 8%.

OCIS codes: (190.4180) Multiphoton processes; (190.7110) Ultrafast nonlinear optics.

References and links

1. A. S. Alnaser, X. M. Tong, T. Osipov, S. Voss, C. M. Maharjan, B. Shan, Z. Chang, and C. L. Cocke, "Laser peak intensity calibration using recoil-ion momentum imaging," Phys. Rev. A **70**, 023413 (2004).
2. A. L'Huillier, L. A. Lompre, G. Mainfray, and C. Manus, "Multiply charged ions induced by multiphoton absorption in rare gases at 0.53 μm," J. Phys. B **16**(8), 1363–1381 (1983).
3. M. D. Perry, O. L. Landen, and A. Szöke, "Measurement of the local laser intensity by photoelectron energy shifts in multiphoton ionization," J. Opt. Soc. Am. B **6**, 344–349 (1989).
4. S. Augst, D. Strickland, D. D. Meyerhoffer, S. L. Chin, and J. H. Eberly, "Tunneling ionization of noble gases in a high intensity laser field," Phys. Rev. Lett. **63**, 2212–2215 (1989).
5. R. Wiehle, B. Witzel, H. Helm, and E. Cormier, "Dynamics of strong-field above-threshold ionization of argon: comparison between experiment and theory," Phys. Rev. A **67**, 063405 (2003).
6. S. M. Hankin, D. M. Villeneuve, P. Corkum, and D. M. Rayner, "Intense-field laser ionization rates in atoms and molecules," Phys. Rev. A **64**, 013405 (2001).
7. A. Staudte, C. Ruiz, M. Schöffler, S. Schössler, D. Zeidler, T. Weber, M. Meckel, D. M. Villeneuve, P. B. Corkum, A. Becker, and R. Dörner, "Binary and recoil collisions in strong field double ionization of helium," Phys. Rev. Lett. **99**, 263002 (2007).
8. M. R. Thompson, M. K. Thomas, P. F. Taday, J. H. Posthumus, A. J. Langley, L. J. Frasinski, and K. Codling, "One and two-colour studies of the dissociative ionization and coulomb explosion of h_2 with intense ti:sapphire laser pulses," J. Phys. B **30**, 5755–5772 (1997).
9. N. B. Delone and V. P. Krainov, *Multiphoton Processes in Atoms*, 2nd ed. (Springer-Verlag, 2000).
10. P. B. Corkum, N. H. Burnett, and F. Brunel, "Above threshold ionization in the long-wavelength limit," Phys. Rev. Lett. **62**, 1259-1262 (1989).
11. N. B. Delone and V. P. Krainov, "Energy and angular electron spectra for the tunnel ionization of atoms by strong low-frequency radiation," J. Opt. Soc. Am. B **8**, 1207–1211 (1991).
12. C. Smeenk, L. Arissian, A. Staudte, D. M. Villeneuve, and P. B. Corkum, "Momentum space tomographic imaging of photoelectrons," J. Phys. B **42**, 185402 (2009).
13. L. Arissian, C. Smeenk, F. Turner, C. Trallero, A. V. Sokolov, D. M. Villeneuve, A. Staudte, and P. B. Corkum, "Direct test of laser tunneling with electron momentum imaging," Phys. Rev. Lett. **105**, 133002 (2010).

#141747 - $15.00 USD Received 27 Jan 2011; revised 18 Mar 2011; accepted 19 Mar 2011; published 28 Apr 2011

14. H. Akagi, T. Otobe, A. Staudte, A. Shiner, F. Turner, R. Dörner, D. M. Villeneuve, and P. B. Corkum, "Laser tunnel ionization from multiple orbitals in HCl," Science **325**, 1364–1367 (2009).
15. R. Dörner, V. Mergel, O. Jagutzki, L. Spielberger, J. Ullrich, R. Moshammer, and H. Schmidt-Böcking, "Cold target recoil ion momentum spectroscopy: a momentum microscope to view atomic collision dynamics," Phys. Rep. **330**, 95–192 (2000).
16. A. Eppink and D. Parker, "Velocity map imaging of ions and electrons using electrostatic lenses," Rev. Sci. Instruments **68**, 3477 (1997).
17. M. V. Ammosov, N. B. Delone, and V. P. Krainov, "Tunnel ionization of complex atoms and of atomic ions in an alternating electromagnetic field," Sov. Phys. JETP **64**, 1191–1194 (1986).
18. S. Augst, D. D. Meyerhoffer, D. Strickland, and S. L. Chin, "Laser ionization of noble gases by coulomb-barrier suppression," J. Opt. Soc. Am. B **8**, 858–867 (1991).
19. F. Krausz and M. Ivanov, "Attosecond physics," Rev. Mod. Phys. **81**, 163-234 (2009).
20. P. R. Bevington and D. K. Robinson, *Data Reduction and Error Analysis for the Physical Sciences*, 2nd ed. (McGraw-Hill, 1992).

Highly nonlinear phenomena, now routinely accessible with the easy availability of femtosecond, intense laser pulses, are by their very nature exquisitely sensitive to intensity. Hence, the knowledge of the intensity in a focused ultrashort laser pulse is crucial for quantitative comparisons of experiment with theory. However, the accurate determination of the intensity is challenging. The traditional way of calculating the intensity from observables of the laser beam itself, such as the pulse energy, and the spatial and temporal profiles, is subject to many errors that quickly add up to a 50% uncertainty in the intensity [2]. On the other hand, a much more accurate intensity calibration can be achieved by exploiting well-understood nonlinear processes, for example, the Stark-shifted resonances in the photoelectron energy spectrum [3–5], or the saturation intensity of the single ionization yield in noble gases [6]. During the last decade the photoion momentum distribution in linearly and circularly polarized light has become a common observable for *in-situ* intensity calibration [1, 7]. In practice, the branching ratio of the dissociation channels in H_2 or D_2 has been used for an empirical intensity calibration [1, 8]. However, this method is reliable only if the pulse duration, wavelength and polarization are identical with respect to the reference intensity calibration.

We have developed an improved model to determine the peak intensity from the photoelectron and photoion momentum distributions in circular polarization. Experimentally, we use both velocity map imaging and cold target recoil ion momentum spectroscopy (COLTRIMS) to test the the quality of our intensity measurement. Our model includes both spatio-temporal integration over a focused Gaussian mode and the atomic physics governing photoionization in strong laser fields. We show that the intensity distribution in the finite focal volume can be replaced with a single value for the peak intensity due to the nonlinearity of multiphoton ionization. We also show that, as long as the intensity is maintained below saturation of single ionization, the retrieved intensity and the quality of the fit is insensitive to spatio-temporal averaging.

Strong field ionization using intense, infrared pulses is often approximated by tunneling [9]. The quantitative model describing strong field ionization in circularly polarized infrared light [10] can be broken into two steps: First, the electron tunnels in the electric field of the laser pulse from its bound state into the classically allowed region. Second, after being separated from the ion, the electron responds classically to the light field. To make the model complete, the classical equations of motion require initial conditions for the tunneled electron wavepacket. These can be derived from a widely accepted model of laser tunnel ionization [11]. However, here we will make use of the fact that the nascent momentum distribution can be measured directly [12, 13].

The attraction of this approach is that the electron receives a classical momentum in the plane of the laser field that is directly proportional to the electric field at the moment of ionization. This momentum is mapped onto the field strength by $p = qE_b/\omega$ where q is the elementary charge, E_b is the laser electric field at the moment of birth and ω is the angular frequency of

#141747 - $15.00 USD Received 27 Jan 2011; revised 18 Mar 2011; accepted 19 Mar 2011; published 28 Apr 2011

the light [10]. Quantum mechanical uncertainty in the initial momentum of the electron will add or subtract from this value in the plane of polarization but it alone contributes in the k direction. Thus, by measuring the electron momentum in two directions simultaneously, we experimentally evaluate the quantum uncertainty and also the laser field strength at the moment of electron birth.

In both electron and recoil ion momentum spectroscopy experiments we used an 800 nm, circularly polarized light pulse produced in a Ti:sapphire regenerative amplification laser system. The laser system produced 2.5 mJ pulses at 1 kHz repetition rate and 50 fs pulse duration. The beam was focused by a 50 mm focal length mirror with an F-number ≈ 12. We used a polarizing beam splitter and power meter to determine the ellipticity with an accuracy of 4%. For the ion experiment we used H_2^+ [1]. However, intensity calibration using COLTRIMS can be performed on any atom or molecule provided sufficient resolution in the single ion can be achieved [7,14]. For the photoelectron experiment, the pulses were first spectrally broadened in a hollow fiber and then compressed to 15 fs using chirped mirrors. The shorter pulses were used to ionize Ar and the photoelectron momentum spectrum was measured. Using a short pulse is not essential for applying our method. The method is general enough to apply to a range of pulse durations and intensities.

To model the laser pulse we assume a Gaussian mode propagating along the z axis with peak intensity I_0 [1]. The beam spot size is $w^2(z) = w_0^2\left(1+z^2/z_0^2\right)$, where w_0 is the $1/e$ beam radius in intensity, and z_0 is the Rayleigh range. The temporal pulse envelope is $f(t) = \exp\left(-4\ln(2)\,t^2/\tau^2\right)$, where τ is the temporal full-width-half-maximum (FWHM) in intensity.

The laser beam was focused into a supersonic gas jet, which was produced in a differentially pumped source chamber and skimmed in y and z to about 0.5 mm in diameter. With a Rayleigh length of $z_0 = 100\ \mu$m the focus was well contained within the 0.5 mm gas jet. We estimate the uncertainty in the lateral momentum to be 10^{-5} atomic units (a.u.), much less than the electron or ion momentum from the femtosecond laser field. A sketch of the experiment illustrating the co-ordinate system used is shown in Fig. 1.

For the photoion measurement we employed COLTRIMS [15]. A constant electric field of $\approx$2 V/cm accelerates the H_2^+ ions towards a commercial detector consisting of micro-channel plate (MCP) and delay line anode (www.roentdek.com). The detector resolves the ion time-of-flight and impact position. This information gives the full momentum 3-vector of each ion. The small DC electric field used in this experiment is not strong enough to keep high velocity ions on the detector, however, it yields an improved velocity resolution of the H_2^+ ions.

For the photoelectron measurements we used a velocity map imaging (VMI) spectrometer [16]. The spectrometer recorded a 2-D projection of the 3-D photoelectron momentum distribution. Electrons ionized by the laser are accelerated in the spectrometer's inhomogeneous electric field to about 2.5 keV before colliding with the MCP detector (Burle Chevron 3040PS). This is large compared to the kinetic energy absorbed from the laser pulse (10-20 eV) and ensures accurate mapping of the 2-D velocity. The method we discuss in this paper can be applied directly to the measured photoelectron spectrum without any inversion of the data, so we do not use any inversion here. The detector was pulsed using a high voltage switch (Directed Energy GRX-3.0K-H) for 300 ns synchronized with each laser pulse. This removes stray electron signal from the measured spectra. The signal from the detector is recorded by a CCD camera (DVC 1312M) acquiring continuously. The raw photoelectron distributions must be corrected for two effects: MCP sensitivity and dark noise. The processed image P used for analysis is given by $P = (R-D)/(S-D)$ where D is a dark image taken with the laser blocked, S is the measured response of the MCP under homogeneous illumination and R is the raw photoelectron spectrum measured with both the laser and gas source on.

In Fig. 2 we show the full measured momentum spectrum of H_2^+ ions. An inset shows an

#141747 - $15.00 USD Received 27 Jan 2011; revised 18 Mar 2011; accepted 19 Mar 2011; published 28 Apr 2011

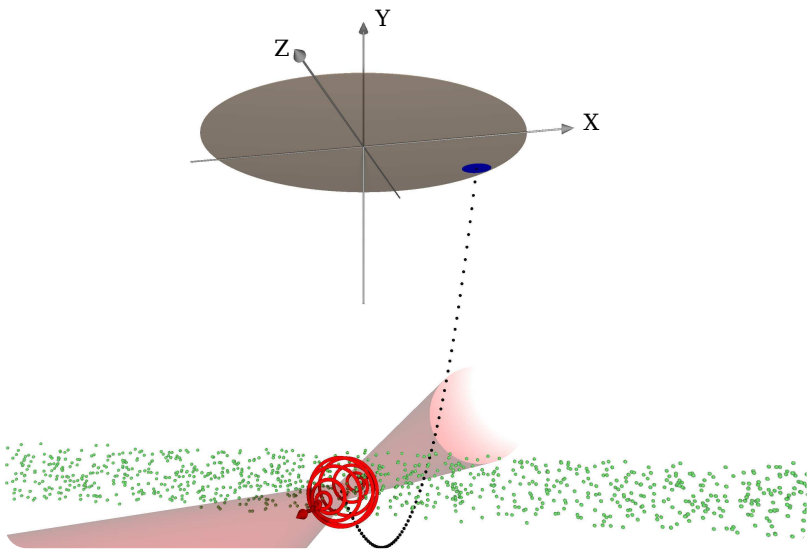

Fig. 1. Schematic view of the experiment. The laser pulse propagates along the z-axis; at the focus, it overlaps the molecular beam, which propagates along x. Charged particles (electrons or ions) are accelerated towards the detector by an electric field parallel to the y axis.

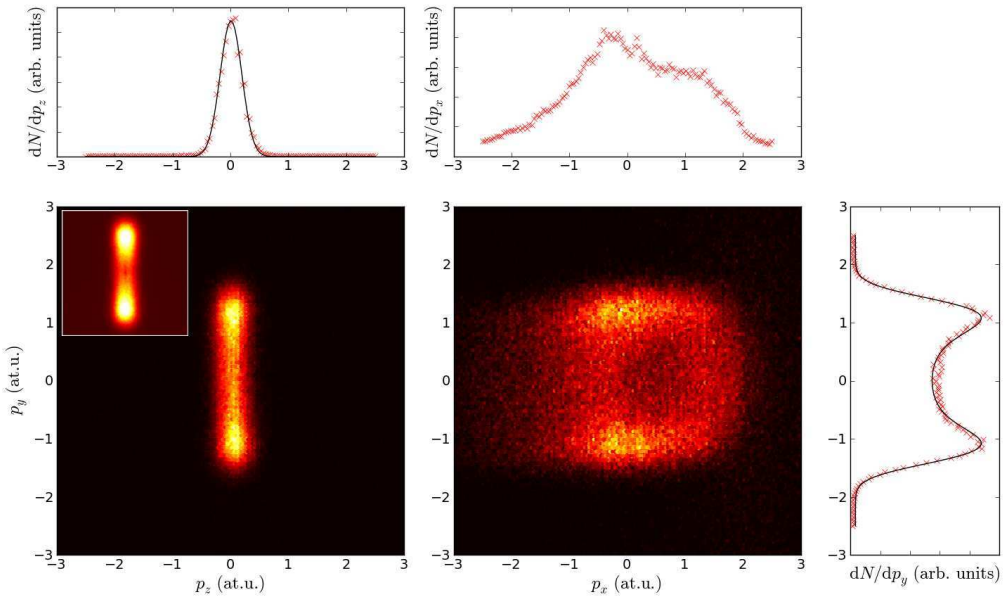

Fig. 2. Two-dimensional projections of 3-D H_2^+ momentum distributions, and their respective integrals. dN/dp_z is the approximately Gaussian curve which gives the quantum uncertainty due to strong field ionization [13]. dN/dp_x is thermally blurred so much information is lost. However, integrating over this direction yields curves with low uncertainty. The inset figure shows a photoelectron momentum spectrum of from Ar ionized under similar laser parameters.

#141747 - $15.00 USD Received 27 Jan 2011; revised 18 Mar 2011; accepted 19 Mar 2011; published 28 Apr 2011

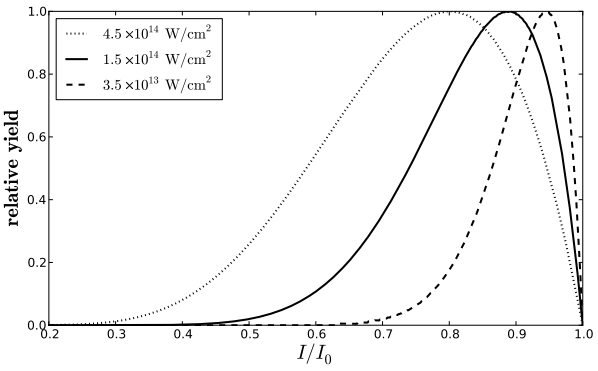

Fig. 3. Relative yield from the laser focus integrated in space and time. The curves correspond to the function in Eq. (1) for three different values of the peak intensity, I_0. The medium was neutral argon ($I_p = 15.76$ eV, $Z = 1$) and the pulse was circularly polarized.

example photoelectron spectrum for comparison. For both electrons and ions the *yz* spectra are very similar indicating the method is applicable to either species. The ion momentum distribution along the gas jet axis (*x*) is blurred by the thermal velocity distribution in the jet. However, the distribution in the *y* direction is not affected and we can obtain a spectrum without thermal blurring by integrating over *x*. The *y* axis corresponds to the time-of-flight axis in the spectrometer. The *xy* plane is the plane of polarization, and therefore the spread of the distribution along the *z* axis is only a result of quantum mechanical effects in strong field ionization [13]. By fitting a Gaussian to the $\mathrm{d}N/\mathrm{d}p_z$ distribution we directly measure the nascent quantum uncertainty in electron or ion momentum. We will show below that an accurate intensity measurement must include this information.

To model the momentum spectrum, we first write the yield from a given iso-intensity shell in the laser focus as

$$\frac{\mathrm{d}N}{\mathrm{d}I} = \left(1 - \exp\left[-\int_{-\infty}^{\infty} W\left[I(t)\right]\mathrm{d}t\right]\right) F(I)\ . \tag{1}$$

In the above, $W(I)$ is the ionization rate function, defined below, and $F(I)$ is given by

$$F(I) \equiv \int_{-\infty}^{\infty} \frac{-\pi z_0 w_0^2}{3} \frac{1}{I^{5/2}} (I_0 f(t) + 2I)(I_0 f(t) - I)^{\frac{1}{2}}\,\mathrm{d}t. \tag{2}$$

Note that Eq. 1 includes saturation of the first ionization state only. Examples of the relative yield from the laser focus are shown in Fig. 3. The curves are examples of Eq. (1) for several different peak intensity values (I_0). The field free I_p of argon was used and $Z = 1$. Only by working well below the saturation intensity [6] does the average intensity in the focus approach the peak intensity, I_0. This makes the method an accurate measurement of the laser pulse.

We use ADK-ionization theory [17] to find the ionization rate function $W(I)$:

$$W(I) \propto I^{C_1} e^{\frac{-C_2}{\sqrt{I}}}, \tag{3}$$

where $C_1 = \left(1 - 2Z/\sqrt{2I_P}\right)/2$, and $C_2 = (2I_P)^{3/2}2/3$. In the above, $Z \equiv 1$ is the charge number, taken as 1 because single ionization is the most likely [18], and I_p is the first ionization energy of the molecule in consideration. Thus C_1 and C_2 are material-dependent constants, not free parameters. Equation (3) is in atomic units (a.u.) and assumes the identity $I = E^2$, which is

#141747 - $15.00 USD Received 27 Jan 2011; revised 18 Mar 2011; accepted 19 Mar 2011; published 28 Apr 2011

widely used in the ultrafast laser community [1, 19]. [Strictly speaking, this relation is not consistent with the canonical definition of atomic units: $e = \hbar = m_e = 4\pi\varepsilon_0 = 1$. The common approach is to convert to SI units via $I_{SI} = 3.5094 \times 10^{16}$ W/cm^2 $\cdot$ E^2_{atomic}, however, this is only correct for linearly polarized light. For a circularly polarized pulse the same identity can be used with the conversion $I_{SI} = 7.019 \times 10^{16}$ W/cm^2 $\cdot$ E^2_{atomic}.]

Using the model it is possible to define the average intensity at which ionization occurs:

$$I_{avg} = \frac{1}{N}\int_0^{I_0} I \frac{\mathrm{d}N}{\mathrm{d}I}\,\mathrm{d}I. \tag{4}$$

This intensity includes integration over the focal volume and pulse duration. This is the most meaningful intensity to use when looking for intensity-dependent features in the momentum spectra (e.g. Freeman resonances [5], or lateral momentum distribution [13]).

The next step is to relate $\mathrm{d}N/\mathrm{d}I$ to the ion or electron drift momentum. Following Refs. [12, 13], we model the momentum distribution in circularly polarized light as a torus:

$$h(I,p) = \frac{1}{\sigma\sqrt{\pi}} \exp\left[-\left(p - \frac{\sqrt{I}}{\omega} \right)^2 / \sigma^2 \right], \tag{5}$$

where σ^2 is the width of the lateral momentum distribution and p is the drift momentum of the tunnel-ionized electron after the pulse has passed. The width σ^2 is the quantum uncertainty from strong field ionization, and it can be measured directly by fitting to the $\mathrm{d}N/\mathrm{d}p_z$ spectrum as shown in Fig. 2. Taking the limit $\sigma \to 0$ in Eq. (5) we obtain the classical expression for the photoelectron or photoion drift momentum: $h(I,p) = \delta\left(p - \sqrt{I}/\omega\right)$. This was used in ref. [1]. We will show that rather than taking $\sigma = 0$, measuring it along the z axis offers a much better fit to experimental observations.

Eq. (5) is then convolved with the yield from each iso-intensity shell to give the final momentum distribution. Thus $\mathrm{d}N/\mathrm{d}p$ is found by

$$\frac{\mathrm{d}N}{\mathrm{d}p} = \int \frac{\mathrm{d}N}{\mathrm{d}I} h(I,p)\,\mathrm{d}I. \tag{6}$$

Strictly speaking, the size σ of the lateral distribution of the photoelectron or photoion depends weakly on intensity [13]. However using a single average value for the lateral distribution over all iso-intensity shells does not significantly affect the results of the model.

To compare with ion spectra or 2-D electron spectra, we must integrate over p_x, which is the molecular beam's propagation direction. For ions, this cancels thermal blurring. Thus,

$$\frac{\mathrm{d}N}{\mathrm{d}p_y} = \int\int \frac{\mathrm{d}N}{\mathrm{d}I} h(I,p)\,\mathrm{d}I\,\mathrm{d}p_x \tag{7}$$

represents the curve that can be measured with high accuracy, and will be fitted to experimentally obtained momentum distributions. Eq. (7) is the Abel transform of Eq. (6).

In Fig. 4 we compare four curves corresponding to slightly modified versions of the model presented above. Each curve represents the best fit to a measured photoelectron spectrum for argon at 800 nm, 2.6×10^{14} W cm^{-2}. Curve (a) is the full model including volume and time integration (a 15 fs pulse was used), and the lateral distribution $h(I,p)$. Curve (b) includes the lateral distribution but does **not** include volume or time integration. This is achieved by setting $\mathrm{d}N/\mathrm{d}I = \delta(I - I_{avg})$ in Eq. (6). Thus model (b) gives the electron a momentum distribution characterized with a single effective laser intensity. Curve (c) is the predicted momentum distribution including volume and time integration, but **not** including the lateral distribution. This

#141747 - $15.00 USD Received 27 Jan 2011; revised 18 Mar 2011; accepted 19 Mar 2011; published 28 Apr 2011

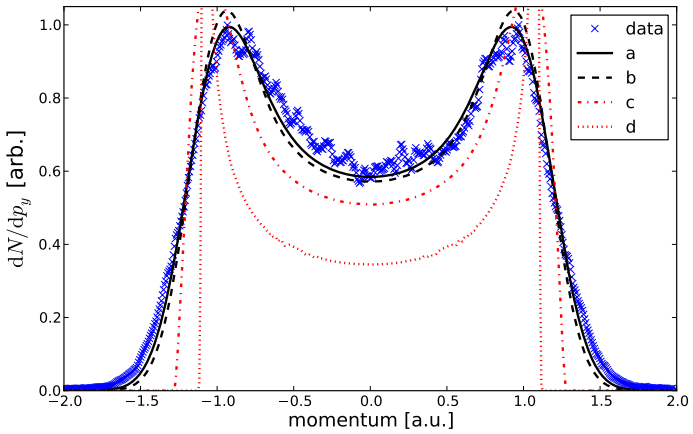

Fig. 4. Calculated momentum distributions fit to Ar photoelectron spectra at 2.6×10^{14} W/cm^2. Curve labels: (a) Model including the lateral distribution, volume and time integration; (b) with lateral distribution, without volume or time integration; (c) with volume and time integration, without lateral distribution; (d) without volume or time integration or lateral distribution.

means taking $\lim \sigma \to 0$ in Eq. (5). Curve (c) is therefore the model of Ref. [1] when the field free I_p and $Z = 1$ are used. Lastly, curve (d) is the result of a model using only the classical expression for the particle's momentum $h(I,p) = \delta\left(p - \sqrt{I}/\omega\right)$ without any lateral distribution or spatio-temporal integration. In this case, Eq. (7) has an analytical solution,

$$\frac{\mathrm{d}N}{\mathrm{d}p_y} = \begin{cases} A\dfrac{\sqrt{I_{avg}}/\omega}{\left(I_{avg}/\omega^2 - p_y^2\right)^{1/2}} & |p_y| < \sqrt{I_{avg}}/\omega \\ 0 & \text{else} \end{cases} \tag{8}$$

where A and I_{avg} are the fitting parameters.

We note that the two curves including the lateral distribution are very similar. Both closely resemble the measured spectrum. The curves that do not include the lateral distribution are considerably more sharp – even if spatio-temporal integration is included. In the following we show that the lateral distribution is critical for achieving an accurate fit to measurements. We will show that the full model (a) is the best fit, however, model (b) which ignores spatio-temporal integration and uses a single value for the laser intensity is almost as good.

For the H_2^+ experiment, three parameters were used for fitting $\mathrm{d}N/\mathrm{d}p_y$: intensity I, a constant offset B to compensate for background signal, and peak height A to account for gas density, detector efficiency and experimental yield.

$$F(p_y) = A\frac{\mathrm{d}N}{\mathrm{d}p_y}(I) + B. \tag{9}$$

The experiment collecting photoelectrons used only the two fit parameters I and A; the background was taken as $B \equiv 0$. The fitting procedure uses the simplex nonlinear optimization algorithm to minimize the value of the reduced χ^2 function by varying the fitting parameters. All other values in the algorithm are measured or known (e.g. wavelength, pulse length, I_p, Z). The goodness of fit is evaluated by the magnitude of the reduced χ^2 [20].

In Fig. 5 we show how the relation between pulse energy and intensity scales. Below saturation the intensity increases linearly with pulse energy. Once saturation is reached the momentum

#141747 - $15.00 USD Received 27 Jan 2011; revised 18 Mar 2011; accepted 19 Mar 2011; published 28 Apr 2011

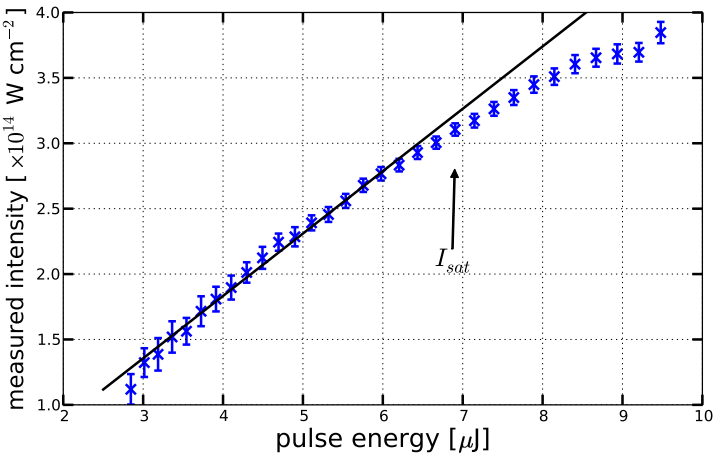

Fig. 5. Relation between pulse energy and measured peak intensity for the electron experiment (15 fs pulse). At low pulse energy the intensity increases linearly with energy. Once saturation is reached, the relationship deviates from linear.

distribution continues to broaden but deviates from the original line.

By fitting to momentum spectra recorded at several different laser intensities we can quantify the accuracy of the fit and identify the relative importance of spatio-temporal averaging and the lateral distribution. At each intensity a photoelectron spectrum was recorded and the four different models were fit to the measurement. The resulting reduced χ^2 values are shown in Fig. 6. In Fig. 6 there are data markers for each of the four models. The reduced χ^2 for model (a), including the volume and time integration and lateral momentum distribution, is shown as the blue circles. Model (b), including the lateral distribution but not including spatio-temporal integration, is shown as the green $\times$ markers and is slightly larger than model (a). However, the reduced χ^2 values are still quite small for model (b). Also shown are models (c) and (d) as the red triangles and green squares. Models (c) and (d) do not include the lateral distribution and have considerably larger χ^2 values.

Fig. 6 shows that the best fit – that is, the smallest χ^2 – is obtained for the full model (a). However, model (b) is very close. Models (c) and (d) which do not include the lateral distribution have substantially larger reduced χ^2. This is consistent with Fig. 4 where it is clear that curves (a) and (b) much more closely resemble the measured spectrum.

The agreement of models (a) and (b) illustrates the importance of including the lateral distribution (i.e. the quantum uncertainty) in fitting to the longitudinal momentum distribution. The complete model including the lateral distribution and spatio-temporal integration is the most accurate fit. By comparing the increase in χ^2 for model (b) to the increase for model (c), we observe that the lateral distribution is of more significance than spatio-temporal averaging. The result for model (b) shows that the distributions can be accurately described by a single laser intensity – ignoring spatio-temporal averaging – provided the quantum mechanical lateral distribution is included.

The goodness of fit is further explained in the inset to Fig. 6. This shows an example of the reduced χ^2 function for a single spectrum recorded at 2.55×10^{14} W cm^{-2}. The inset shows the value of the optimization parameter χ^2 as a function of the intensity I used to fit the distribution via Eq. (9). In the inset the intensity is a fitting parameter. It is assumed the minimum χ^2 corresponds to the true intensity value. We see that the minimum χ^2 value occurs for model (a) as expected. Model (b) is a slightly less good fit. Models (c) and (d) are poor fits

#141747 - $15.00 USD Received 27 Jan 2011; revised 18 Mar 2011; accepted 19 Mar 2011; published 28 Apr 2011

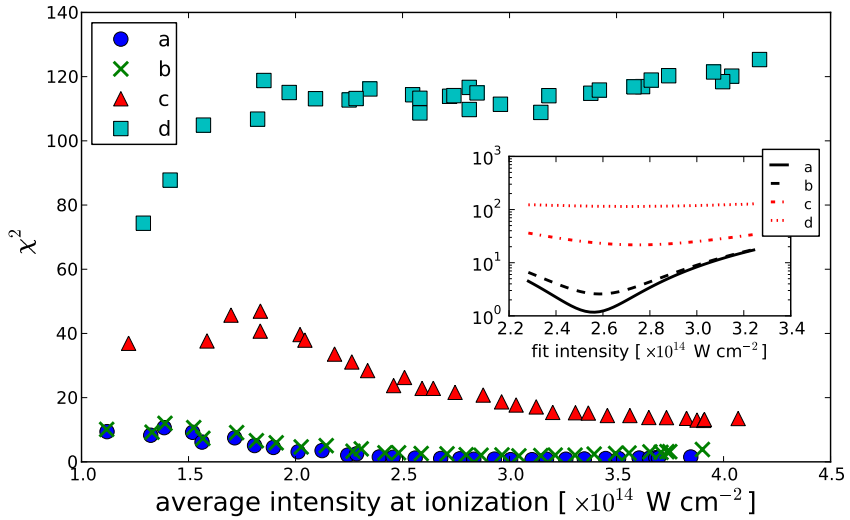

Fig. 6. Goodness of fit for Ar at 800 nm over a range of laser intensities. The reduced χ^2 statistic is shown for fitting with different models. Inset: Example χ^2 function for a single spectrum at 2.55×10^{14} W cm^{-2}. Model labels: (a) With lateral distribution, volume and time integration; (b) with lateral distribution, without volume or time integration; (c) with volume and time integration, without lateral distribution; (d) without volume or time integration or lateral distribution.

and have χ^2 values larger by an order of magnitude or more. The substantially larger value of χ^2 for the models that do not include the lateral distribution illustrates that the lateral distribution is more significant than spatio-temporal averaging. Comparing curves (a) and (b), we see that curve (a) has a very well defined minimum compared to model (b). This is consistent with the results in the main figure. For spectra containing more than 10^5 photoelectrons, we estimate the precision of the fit using model (a) is 4% in intensity. Similar results are obtained for fits to other measured spectra. The complete model (a) is the most precise intensity measurement.

In addition to the uncertainty in the the fit, there are other experimental uncertainties associated with momentum calibration (2% in σ and 4% in I), laser ellipticity (4% in I), detector sensitivity (1% in σ), and chamber alignment (1% in σ). When combined with the fit uncertainty, the total accuracy of the intensity measurement is 8%.

In conclusion, strong field ionization with circularly polarized light provides an accurate and sensitive method for measuring the intensity of ultrashort pulses. The pulse must be short enough that the charged particle does not move significantly in the focus. The method can be applied to any gas medium that ionizes in intense fields and works with both positive and negative charged particle detectors. It is roubust, and independent of complex molecular fragmentation dynamics that occur in the presence of the strong laser fields. The intrinsic uncertainty of the best model presented here is approximately 4%. We estimate the total uncertainty of the measurement, including systematic errors to be approximately 8%.

Acknowledgements

CTH acknowledges a NSERC postdoctoral fellowship. CS acknowledges a NSERC postgraduate fellowship. We are pleased to acknowledge funding from NSERC, the Canadian Institute for Photonics Innovations and MURI grant W911NF-07-1-0475.

#141747 - $15.00 USD Received 27 Jan 2011; revised 18 Mar 2011; accepted 19 Mar 2011; published 28 Apr 2011